Wind and Structures, Vol. 15, No. 3 (2012) 189-208
DOI: http://dx.doi.org/10.12989/was.2012.15.3.189

Lock-in and drag amplification effects in slender line-like structures through CFD

Ali Vasallo Belver*[1], Antolín Lorenzana Ibán[1,2] and Riccardo Rossi[3]

[1]*CARTIF Centro Tecnológico, Parque Tecnológico de Boecillo, parcela 205, 47151 Boecillo (Valladolid), Spain*
[2]*ITAP. University of Valladolid, Paseo del Cauce 59, 47011 Valladolid, Spain*
[3]*International Center for Numerical Methods in Engineering, Barcelona, 08034, Spain*

(Received November 11, 2010, Revised June 30, 2011, Accepted July 17, 2011)

Abstract. Lock-in and drag amplification phenomena are studied for a flexible cantilever using a simplified fluid-structure interaction approach. Instead of solving the 3D domain, a simplified setup is devised, in which 2D flow problems are solved on a number of planes parallel to the wind direction and transversal to the structure. On such planes, the incompressible Navier-Stokes equations are solved to estimate the fluid action at different positions of the line-like structure. The fluid flow on each plane is coupled with the structural deformation at the corresponding position, affecting the dynamic behaviour of the system. An Arbitrary Lagrangian-Eulerian (ALE) approach is used to take in account the deformation of the domain, and a fractional-step scheme is used to solve the fluid field. The stabilization of incompressibility and convection is achieved through orthogonal quasi-static subscales, an approach that is believed to provide a first step towards turbulence modelling. In order to model the structural problem, a special one-dimensional element for thin walled cross-section beam is implemented. The standard second-order Bossak method is used for the time integration of the structural problem.

Keywords: fluid-structure interaction; vortex-induced vibrations; slender line-like structures; lock-in; drag coefficient amplification

1. Introduction

Multidisciplinary problems involving the interaction between fluids and structures are common in engineering design. Essentially, fluid structure-interaction (FSI) phenomena are caused by the forces exerted from the flow around a structure resulting in a deformation of the structural domain, which in turns alters the flow in a dynamic manner. In particular, vibrations generated by vortex shedding are of practical interest in many fields of engineering. Structures such as bridges, industrial chimneys, tall buildings or cables are designed according to aeroelastic criteria (Repetto 2002, Nieto 2010).

The significance of vortex-induced vibrations (VIV) has led to a considerable amount of research work, either experimental or theoretically, the latter through nonlinear-oscillator modelling approaches and, recently, also through Computational Fluid Dynamics (CFD). In the comprehensive review of Williamson and Govardhan (2008) fundamental results and discoveries concerning VIV are discussed.

* Corresponding author, Dr., E-mail: alivas@cartif.es

Various 2D analytical vortex shedding models have been used in the analysis of vibrations. Some of them have been developed for the analysis of the response in the lock-in region and consider the vortex-shedding force as a sine function, using adjusted coefficients and parameters, and considering that the response in this region is almost harmonic (Kwok 1981). Other authors use the random vibration theory to evaluate the structure response, considering this force as a Gaussian function. The model of Vickery and Clark (1972), applied to towers, can be considered included in this type, and it has been used by other researchers (Hansen 1981) to compare its results with experimental outcomes, obtaining satisfactory results.

Semi-empirical models have also been developed to research the vortex shedding forces in cylinders, taking into account the spatial correlation between these forces, that depend on the amplitude, and considering the phenomenon as a random, stationary, narrow-band process, with high Reynolds numbers (Blevins 1976).

The intrinsic nature of vortex-induced vibrations suggests that the fluid behaviour can also be modelled as a nonlinear oscillator. This idea was initially proposed by Bishop and Hassan (1964) and followed by other researchers (Hartlen 1970, Skop 1975), using models where the lift coefficient (for horizontal cylinders) or the lateral force coefficient (for vertical cylinders) satisfy a van der Pol type equation. In their model, a van der Pol soft nonlinear oscillator for the lift force is coupled to the cylinder motion by a linear dependence on the cylinder velocity. The cylinder motion is restricted just to translation in the transverse direction, perpendicular to both the flow direction and the cylinder axis. The cylinder is restrained by linear springs and is linearly damped.

Considering the idea of an auto-excited oscillator, Simiu and Scanlan (1978) presented two empirical models to simulate the vortex shedding force in rigid bodies: one of them linear, in which exciting, damping and rigidity parameters were considered, and the other one nonlinear, with the aeroelastic force parameters depending on the velocity and displacement of the structure. Other accepted approaches are based on the van der Pol equation, for example, in the specific case of towers, the model of Vickery and Basu (1983). This model, including some complements, was used in the works of Gorski (2008, 2009) to study the along and across-wind response of tall industrial chimneys due to the vortex excitation. One of the hypotheses used in other models (Skop and Luo 2001) is that the excitation force depends on the structure response, mainly on the velocity (condition that characterizes the aerodynamic damping).

On the other hand, besides these 2D analytical and semi-empirical models for the analysis of vibrations caused by vortex shedding, there are some models based on CFD. Unlike other methods, the numerical methodology used to solve aeroelastic problems in structural engineering is characterized by no requirement for experimental data, although model updating techniques should be used.

The first numerical researches on air flow around a cylinder were carried out by Son and Hanratty (1969). Also Braza *et al*. (1986) used the finite volume method to analyse the vortex shedding in cylinders, with a Reynolds number less than 1000. Later, Dawes (1993) used the finite volume method to solve the same problem. He used an adaptive method, including the ability of refining the mesh in function of the solution obtained, to get a computationally economical solution. Kalktsis *et al*. (2007) used the spectral element method to carry out a computational research of the forces on a cylinder harmonically oscillating in a perpendicular direction to the uniform flow. Other authors, like Jan and Sheu (2004) and Mittal *et al*. (2006, 2008), have also used the finite element method to analyse the vortex shedding phenomenon.

Lucor *et al*. (2001) investigated very-long bodies (aspect ratio > 500) in uniform and sheared flows to observe vortex dislocations with similar appearance to that found in fixed-body flows,

which cause substantial modulation of lift forces. Willden and Graham (2001) developed an efficient "quasi-3D" simulation, where the two-dimensional flow is computed at various spanwise locations, and these are linked by a three-dimensional large-scale vortex lattice representation.

Other researchers, like Rodi (1997) or Lankadasu and Vengadesan (2010), studied the vortex shedding phenomenon for non-aerodynamic bodies. Meneghini *et al*. (2004) used the discrete vortex method to studied vortex-induced vibrations on long flexible cylinders immersed in complex flow fields. The numerical methodology to analyse the lock-in phenomenon, and its relation with the use conditions of slender structures to limit their vibration levels, was used by Lopes *et al*. (2004). In order to analize the air flow and its action on the structure, these researchers used a method based on the finite volumes technique, while the dynamic behaviour of the structure was calculated with the finite element method.

The present work focuses on the case of FSI problems. The structure is assumed to be slender enough that although small strain theory is considered, displacements can be large. Because of this, not only deformed configuration can be significantly different from the undeformed one, but also movements can affect the fluid field, leading to interaction effects. This is the case for e.g. masts and chimneys, and it means that the structure can be accurately modelled with a beam finite element formulation. The fluid (air) is assumed to be incompressible and also no flow is present in the direction of the beam, so that it can be modelled using a certain number of planes orthogonal to the beam axis. The simplifying assumption that the flow on each of the planes is independent on the flow on the neighbouring ones is taken and no tip effects are considered. With these assumptions, VIV are studied by coupling a one-dimensional structural model to the fluid flow using a simplified FSI algorithm. The response of a cantilever beam subjected to the wind action is shown in a range where vibration behaviour is critical, resulting in lock-in and drag amplification phenomena.

The paper is organized as follows. In Section 2 the lock-in and drag amplification phenomena are briefly explained. Section 3 describes the structural model, Section 4 the fluid model and Section 5 the fluid-structure coupling algorithm. In Section 6, the simulation of a steel mast under wind action is carried out and the lock-in and drag amplification phenomena are showed. Finally, Section 7 concludes by summarizing the main aspects of the contributions presented in this paper.

2. Lock-in and drag amplification phenomena

Vortex-induced vibrations occur when vortices are shed alternatively from opposite sides of the structure. The vortex shedding frequency n_s is, according to the Strouhal relation

$$n_s = S_t \frac{U}{d} \tag{1}$$

Where *St* depends mainly upon body geometry and the Reynolds number, d is some across-wind dimension of the body, and U is the mean velocity of the uniform flow in which the body is immersed. This gives rise to a fluctuating force density $F_y(t)$ perpendicular to the wind direction, which can be rendered dimensionless and expressed in terms of lift coefficient as

$$C_L(t) = \frac{F_y(t)}{\frac{1}{2}\rho U^2 d} \tag{2}$$

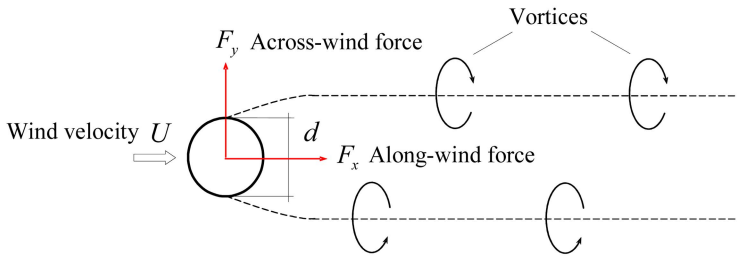

Fig. 1 Vortex shedding (Dyrbye and Hansen 1997)

where ρ is the fluid density. In its most simple form, a stable street of staggered vortices forms behind the structure, see Fig. 1.

Under the action of the vortices shed in its wake the structure will be driven periodically, but this driving will lead only small response unless the vortex shedding frequency approaches the natural across-flow natural frequency of the structure n_e. Near this frequency greater body movement is excited, and the structural motion begins to interact strongly with the flow in such a way that the vortex shedding frequency synchronizes with the natural frequency of the structure, which controls the vortex-shedding phenomenon even when variations in flow velocity modify the nominal Strouhal frequency away from the natural frequency by a few percent. This phenomenon is called lock-in and it is usually observed for low values of mass and/or structural damping (Feng 1968, Vickery 1983).

On the other hand, an interesting large-amplitude response mode is observed at higher velocities outside the principal synchronization range (Fujarra 2001, Kitagawa 1999), resulting in a large amplification of the drag coefficient, which is expressed as

$$C_D(t) = \frac{F_x(t)}{\frac{1}{2}\rho U^2 d} \tag{3}$$

This vibration mode is due to a coupled streamwise-transverse motion, where the streamwise amplitude becomes non-negligible. There is strong correlation between the streamwise and transverse motions, as the frequency of the transverse oscillation is exactly half the frequency for the streamwise vibrations.

3. Structural model

An analytical one-dimensional model was developed to describe the behaviour of 3D thin-walled beams. Detailed description of the model can be seen in the work of Mediavilla *et al*. 2007. Fourteen degrees of freedom are used for each straight beam element (2 nodes) accounting for extension, shearing, bending, bi-moment and torsion. The methodology proposed uses a Love-Kirchoff shell model to relate the stresses and strains in the shell. In this relation are introduced the generalized beam deformations corresponding to the Navier-Bernoulli and Vlasov models through geometric considerations but deformations of the cross-section of the beam as ovalization are not taken into account.

The standard equation of motion is proposed in terms of $\boldsymbol{K}$ (stiffness matrix), $\boldsymbol{M}$ (mass matrix)

and $\boldsymbol{f}_{ext}(z,t)$ (external load vector), where z is the longitudinal coordinate for the beam (and for the line-like structure). Proportional damping is assumed and the damping matrix $\boldsymbol{C}$ is expressed in term of the mass matrix $\boldsymbol{M}$. A second-order accurate Bossak scheme is used in the time integration of the resultant equation of motion

$$\boldsymbol{M}\ddot{x} + \boldsymbol{C}\dot{x} + \boldsymbol{K}x = \boldsymbol{f}_{ext}(z, t) \tag{4}$$

4. Computational *Fluid D*ynamics

For incompressible behaviour, typically accepted in the civil engineering applications, the Navier-Stokes equations can be expressed as

$$\frac{\partial \boldsymbol{v}}{\partial t} + (\boldsymbol{v} \cdot \nabla)\boldsymbol{v} - v\nabla^2\boldsymbol{v} + \nabla p = \boldsymbol{b} \tag{5}$$

$$\nabla \cdot \boldsymbol{v} = 0 \tag{6}$$

The solution procedure is based on a fractional step scheme (Codina 2001), namely, a second order algorithm based on the Crank–Nicolson discretization for the viscous and convective terms and a second order pressure splitting, leaving the pressure gradient at a given time level in the first step and computing its increment in the second one.

The fractional step scheme is described briefly below, in its basic form, without the introduction of any stabilization for the pressure term. The starting point is the spatial discretization of the Navier-Stokes Eqs. (5) and (6). The matrix form of the problem using the Galerkin approach is given by

$$\boldsymbol{M}\frac{\boldsymbol{V}^{n+1} - \boldsymbol{V}^{n}}{\delta t} + \boldsymbol{K}(\boldsymbol{V}^{n+\theta})\boldsymbol{V}^{n+\theta} + \boldsymbol{G}\boldsymbol{P}^{n+1} = \boldsymbol{F}^{n+\theta} \tag{7}$$

$$\boldsymbol{D}V^{n+1} = 0 \tag{8}$$

where $\boldsymbol{V}$ and $\boldsymbol{P}$ are the arrays of nodal velocities and pressures, respectively.

The fractional step scheme is based on the introduction of an auxiliary variable $\tilde{\boldsymbol{V}}^{n+1}$, in terms of which the time derivative can be written as

$$\frac{\boldsymbol{V}^{n+1} - \boldsymbol{V}^{n}}{\delta t} = \frac{\boldsymbol{V}^{n+1} - \tilde{\boldsymbol{V}}^{n+1}}{\delta t} = \frac{\tilde{\boldsymbol{V}}^{n+1} - \boldsymbol{V}^{n}}{\delta t} \tag{9}$$

and the fractional step scheme can be presented as

$$\boldsymbol{M}\frac{\tilde{\boldsymbol{V}}^{n+1} - \boldsymbol{V}^{n}}{\delta t} + \boldsymbol{K}(\boldsymbol{V}^{n+\theta})\boldsymbol{V}^{n+\theta} + \boldsymbol{G}\boldsymbol{P}^{n} = \boldsymbol{F}^{n+\theta} \tag{10}$$

$$\boldsymbol{M}\frac{\boldsymbol{V}^{n+1} - \tilde{\boldsymbol{V}}^{n+1}}{\delta t} + \boldsymbol{G}(\boldsymbol{P}^{n+1} - \boldsymbol{P}^{n}) = 0 \tag{11}$$

$$\boldsymbol{D}V^{n+1} = 0 \tag{12}$$

Using the following approximation

$$\boldsymbol{K}(\boldsymbol{V}^{n+\theta})\boldsymbol{V}^{n+\theta} \approx \boldsymbol{K}(\tilde{\boldsymbol{V}}^{n+\theta})\tilde{\boldsymbol{V}}^{n+\theta} \tag{13}$$

where

$$\tilde{\boldsymbol{V}}^{n+\theta} = \theta\,\tilde{\boldsymbol{V}}^{n+\theta} + (1-\theta)\boldsymbol{V}^{n} \tag{14}$$

and expressing $\mathbf{V}^{n+1}$ in terms of $\tilde{\boldsymbol{V}}^{n+1}$ using Eq. (11) and inserting the result in Eq. (12), the set of equations to be solved is

$$\boldsymbol{M}\frac{\tilde{\boldsymbol{V}}^{n+1}-\boldsymbol{V}^{n}}{\delta t} + \boldsymbol{K}(\tilde{\boldsymbol{V}}^{n+\theta})\tilde{\boldsymbol{V}}^{n+\theta} + \boldsymbol{G}\boldsymbol{P}^{n} = \boldsymbol{F}^{n+\theta} \tag{15}$$

$$\delta t\boldsymbol{D}\boldsymbol{M}^{-1}\boldsymbol{G}(\boldsymbol{P}^{n+1}-\boldsymbol{P}^{n}) = \boldsymbol{D}\tilde{\boldsymbol{V}}^{n+1} \tag{16}$$

$$\boldsymbol{M}\frac{\boldsymbol{V}^{n+1}-\tilde{\boldsymbol{V}}^{n+1}}{\delta t} + \boldsymbol{G}(\boldsymbol{P}^{n+1}-\boldsymbol{P}^{n}) = 0 \tag{17}$$

Note that $\boldsymbol{D}\boldsymbol{M}^{-1}\mathbf{G}$ can be replaced by the Laplacian operator $\boldsymbol{L}$ and hence the fractional step scheme takes the form

- Step A

$$\boldsymbol{M}\frac{\tilde{\boldsymbol{V}}^{n+1}-\boldsymbol{V}^{n}}{\delta t} + \boldsymbol{K}(\boldsymbol{V}^{n+\theta})\boldsymbol{V}^{n+\theta} + \boldsymbol{G}\boldsymbol{P}^{n} = \boldsymbol{F}^{n+\theta} \tag{18}$$

- Step B

$$\delta t\boldsymbol{L}(\boldsymbol{P}^{n+1}-\boldsymbol{P}^{n}) = \boldsymbol{D}\tilde{\boldsymbol{V}}^{n+1} \tag{19}$$

- Step C

$$\boldsymbol{M}\frac{\boldsymbol{V}^{n+1}-\tilde{\boldsymbol{V}}^{n+1}}{\delta t} + \boldsymbol{G}(\boldsymbol{P}^{n+1}-\boldsymbol{P}^{n}) = 0 \tag{20}$$

The fluid solver used in current work was based on the use of Orthogonal Sub-Grid Scale (OSS) stabilization, as described for example in Codina (2000, 2002). Such stabilization falls into the category of Variational Multi-Scale (VMS) techniques, which have been deeply investigated during the last decade. An important property of such techniques is that, aside of allowing a stable Finite Element solution, they tend to introduce a dissipation into the solution that acts similarly to a turbulence model. A mathematical discussion on the effectiveness of such models in modelling the turbulence can be found for example in the work of Codina *et al*. (2010), Principe *et al*. (2010) or Oñate *et al.* (2007), while some empirical evidence of their success in simulating high Reynolds number flows around bluff bodies can be found in the work of Rossi and Oñate. (2010).

Another different, but equally important feature of the numerical method used, is the use of the so-called non-conservative form of the momentum equation. It has been shown recently (see for example, the work of Forster 2007) how solvers based on such approach are much less sensitive to eventual violations of the Geometric Conservation Law than alternatives based on the conservative

form, which is typically used in Finite Volume solvers. In any case, the mesh motion scheme used in the current work guarantees that at least the First-Order Geometric Conservation Law (Selvam *et al*. 2002) is verified.

5. Fluid-structure coupling

To perform the interaction between the structural and fluid problems, it is necessary to identify the geometry of the cross-section of the beam and the distribution of pressure (force density) on its boundary. Under the usual assumptions, the motion of the beam axis describes the motion of the whole cross-section, which can be imagined as a rigid surface which follows the translation and the rotation of the beam axis. Any section of finite dimensions in the xy plane is associated to the corresponding point of the one-dimensional beam element, assumed to be oriented in the Oz axis.

The current work focuses on bluff-bodies, in particular a circular cross-section cylinder subjected to a flow orthogonal to the axis, with a clear predominance of the shape resistance over the friction resistance. In this kind of problem a time-accurate viscous flow solver is needed. Under this assumption, the fluid domain was modelled with a number of independent planes of fluid where the problem can be solved separately. Summarizing, as sketched in Fig. 2, the CFD solution on each fluid plane provides a force density $F_x(t)$ and $F_y(t)$, acting on the cross-section of the beam, which is obtained by integrating the pressure of the fluid $p(\theta, t)$ over the boundary of the cross-section. So, a time-varying distributed load over the structure was obtained by interpolation between consecutive fluid planes.

In this work, the aeroelastic problem is characterized by large Reynolds numbers and flow separation around the circular cross-section. Since the added-mass effect is expected to be low for this kind of problems, the choice of Loose Coupling procedures appears to be convenient (see Rossi and Oñate 2010). The use of tightly coupled schemes (see for example the work of Idelsohn *et al*. (2009)) for the solution of the coupled problem of interest represents, of course, a possible alternative. Nevertheless, such approach would imply increasing the computing time and was not seen as needed given the good performance of the simple coupling scheme used.

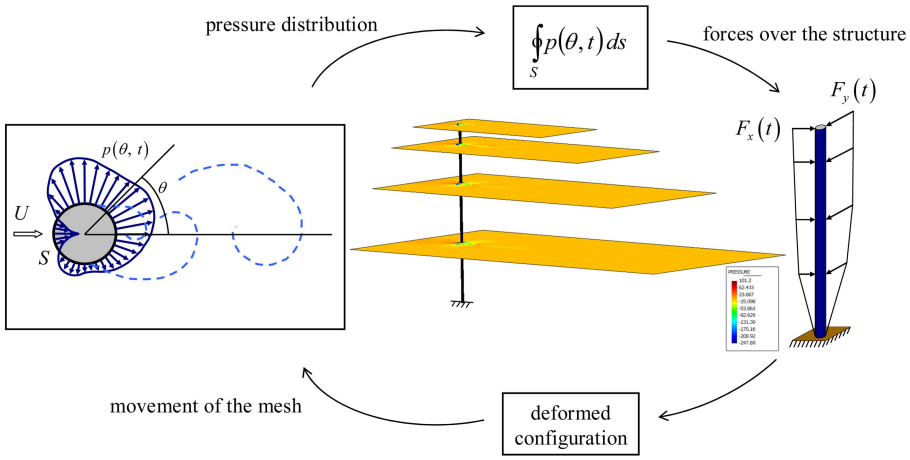

Fig. 2 Overview coupling problem

In this scheme, the structural solution was integrated in the fractional step procedure, and the ALE formulation was used to take into account the movement of the fluid mesh (Donea and Huerta 2003).

The coupling scheme was based on the following steps

1. Solve the structural problem for an initial guess pressure, $\boldsymbol{X}^{*}_{n+1_s} = \boldsymbol{X}^{*}_{n+1_s}(\boldsymbol{P}^{*}_{n+1})$
2. Move the fluid domain according to the structure motion, $\boldsymbol{X}^{*}_{n+1} = \boldsymbol{X}^{*}_{n+1}(\boldsymbol{P}^{*}_{n+1})$
3. Step A, $\tilde{\boldsymbol{V}}^{n+1}$
4. Step B, $\boldsymbol{P}_{n+1}$. Impose pressure boundary conditions
5. Solve the structural problem for the calculated pressure, $\boldsymbol{X}_{n+1_s} = \boldsymbol{X}_{n+1_s}(\boldsymbol{P}_{n+1})$
6. Step C, $\boldsymbol{V}^{n+1}$. Impose velocity boundary conditions

The structural model, the CFD abilities and the former numerical methods have been implemented in Kratos (Dadvand *et al*. 2010), an object-oriented framework for developing finite element codes for multi-disciplinary applications.

6. Steel mast subjected to wind action

The lock-in and drag amplification phenomena were studied for a 34 *m* steel mast under wind action, by coupling the one-dimensional structural model to the fluid flow using a simplified fluid-structure coupling algorithm (Belver *et al*. 2010). The diameter of the mast was $d = 0.5$ *m* and the shell thickness is 4.8 *mm*. The elastic properties were Young's modulus $E = 2.1 \cdot 10^{11}$ *Pa*, Poisson's ratio $\nu = 0.3$ and density $\rho = 7772$ *Kg/m*^{3}. The mast was modelled as a flexible cantilever with 4 beam finite elements. A mass proportional structural damping β_s was assumed. The first three natural frequencies, n_e, were 0.43, 2.78 and 7.8 *Hz*.

For the fluid (air) the density is $\rho = 1.21$ *Kg/m*^{3} and dynamic viscosity $\mu = 1.8 \cdot 10^{-5}$ *Ns/m*^{2}. The influence of the number of fluid planes used to model the wind action was studied by Belver (2009), considering several cases with different fluid planes located at different heights. For this particular case, the along- and across- wind response of the structure was quite similar regardless of the number of fluid planes considered, so just one plane at the tip was used.

Details of the geometry of the fluid domain are given in Fig. 3. The boundary conditions for the fluid problem were the following: traction-free boundary condition at the edge Γ_d, no-slip condition at the

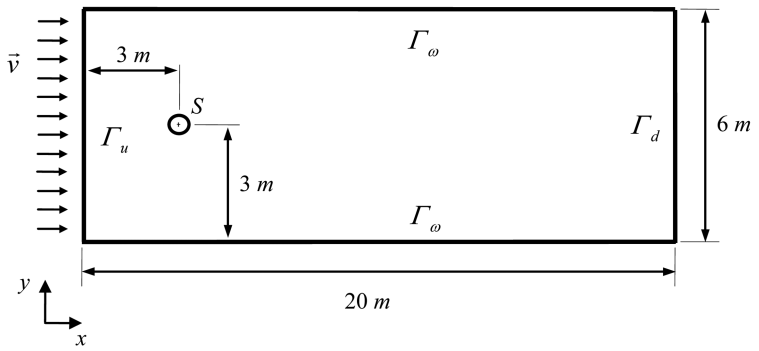

Fig. 3 Boundary conditions definition

cross-section boundary S of the structure, $v_y = 0$ at Γ_ω, and a specified inflow velocity (v_x, 0) at edge Γ_u.

After a mesh convergence study, the fluid plane was meshed according to the sketch in Fig. 4, where the characteristic size is referred to the diameter of the cross-section. A great number of elements were placed near S, the cross-section boundary at the tip, resulting 5846 triangular surface elements. The selected time step was 0.005 s.

This mesh was coarser than the one normally used in CFD. The use of coarse meshes, which is needed to keep reasonably bounded the computational effort, implies a certain error in the determination of along-wind response but appears to be sufficient for the correct representation of the FSI problem. Since the lock-in phenomena is governed mostly by the interaction effects in the across-wind direction, the model described was sufficiently accurate to provide insight in the phenomena, despite the use of a sub-optimal resolution.

6.1 Lock-in phenomenon

The ratios of the vortex shedding frequency to the natural frequency and the amplitude of the across-wind vibration of the structure versus reduced velocity, Eq. (21), are plotted in Figs. 5 and 6. As expected, the lock-in phenomenon only appears for small values for the structural damping (β_s = 0.025). In this particular example, the results in across-wind amplitude for β_s = 0.025 are, for reduced velocities of 5.0 and 5.5, 8 times greater than the corresponding amplitudes for β_s = 0.05 and β_s = 0.075.

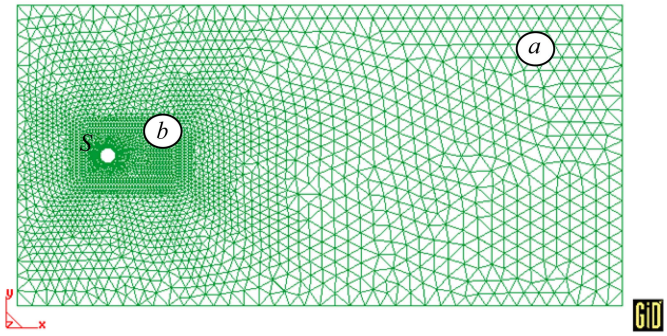

Zone	Characteristic size
a	1
b	1/5
S	1/10

Fig. 4 Fluid domain mesh

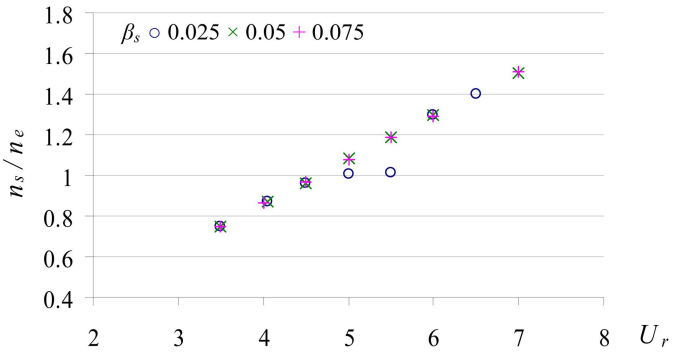

Fig. 5 Frequency response vs. reduced velocity

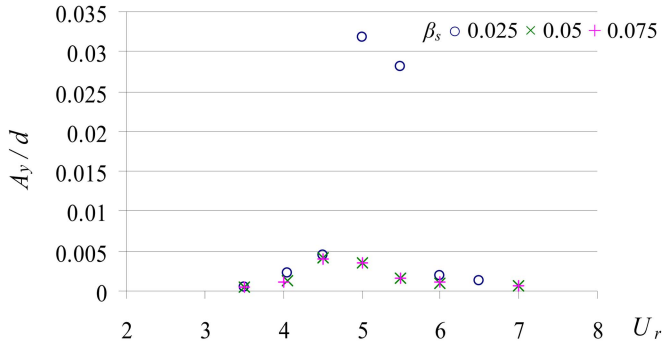

Fig. 6 Amplitude response vs. reduced velocity

$$U_r = \frac{U}{n_e d} \tag{21}$$

Figs. 7 and 8 show the lift coefficient and the across-wind displacement of the structure for β_s = 0.025 and U_r = 5.5, respectively. In the range of interest, from 260 to 1500 *s*, the synchronization between the vortex-shedding frequency and the natural frequency of the structure can be observed. During the first seconds of the analysis (t < 800 *s* approximately), the transverse displacements are small and the lift coefficient is characterized by a root mean square (RMS) value of 0.24 and a frequency of 0.51 *Hz* (Fig. 9). These values agree with those given by Norberg (2001), being the Strouhal number 0.21 and Reynolds number 4.07·104. So, using Eq. (1), n_s = 0.21*1.22/0.5 = 0.51 *Hz*.

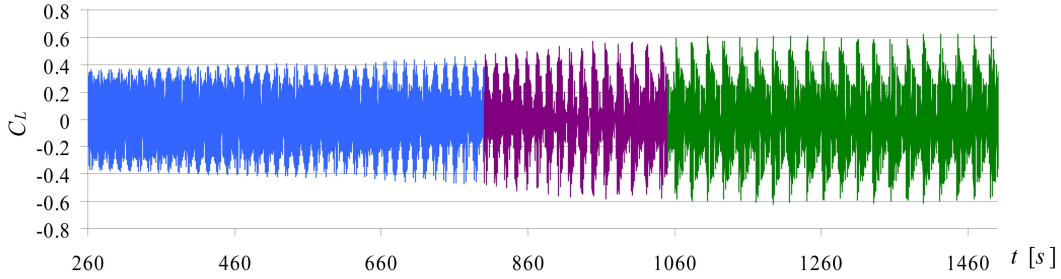

Fig. 7 Lift coefficient vs. time

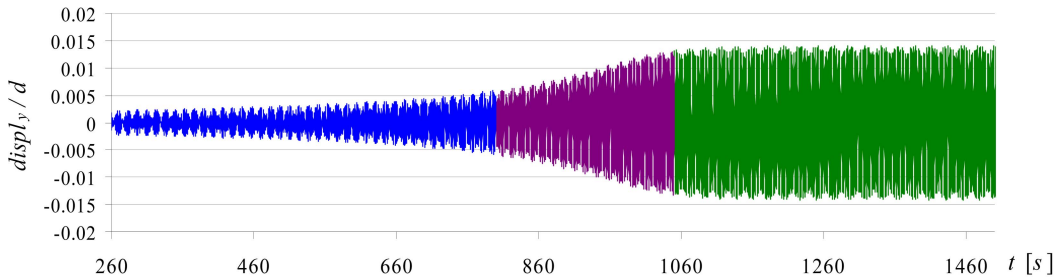

Fig. 8 Across-wind vibration of the structure

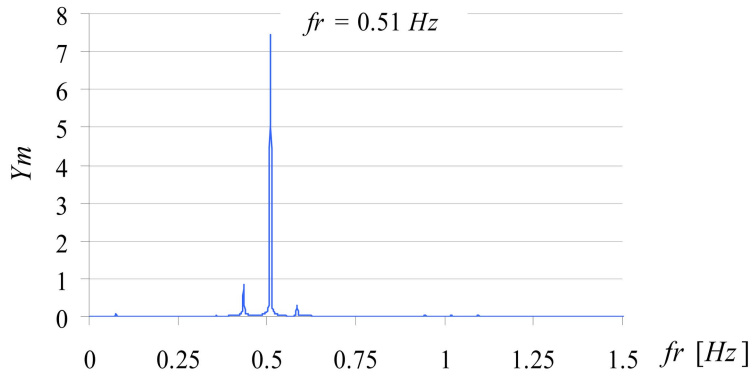

Fig. 9 Power Spectral Density (PSD) for C_L for 260 < t < 800 s

Synchronization between the first natural frequency, n_e and the vortex shedding frequency, n_s occurs in the range 800 – 1000 s (Fig. 10) and for a time t > 1000 s, the frequency of the fluctuating lift coefficient is equal the natural frequency (Fig. 11) and the transverse displacements increase significantly due to the structural motion begins to interact strongly with the wind field and the natural frequency of the structure commands the vortex-shedding phenomenon. Interestingly, the

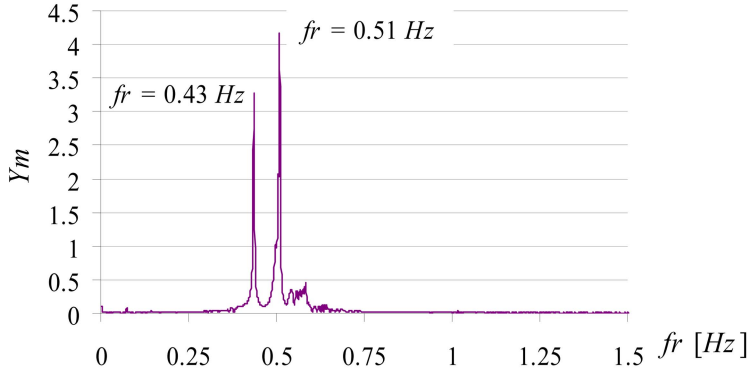

Fig. 10 PSD for C_L for 800 < t < 1000 s

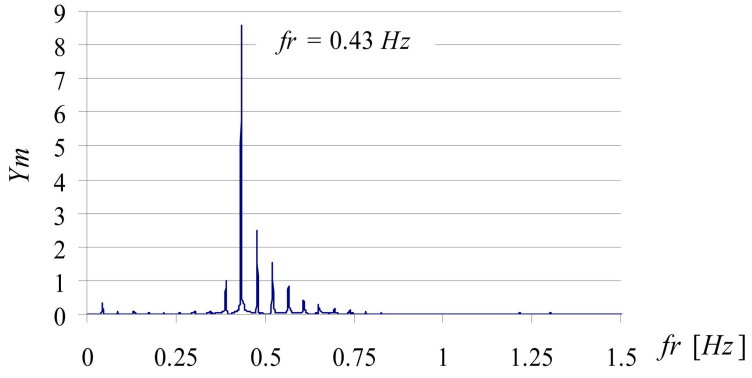

Fig. 11 PSD for C_L for t > 1000 s

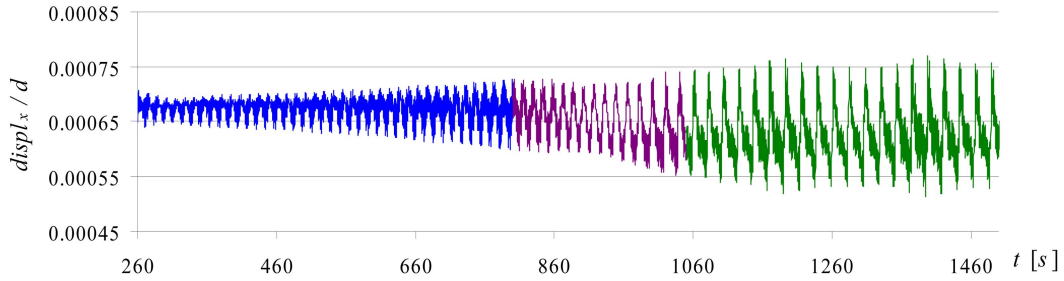

Fig. 12 Along-wind vibration of the structure

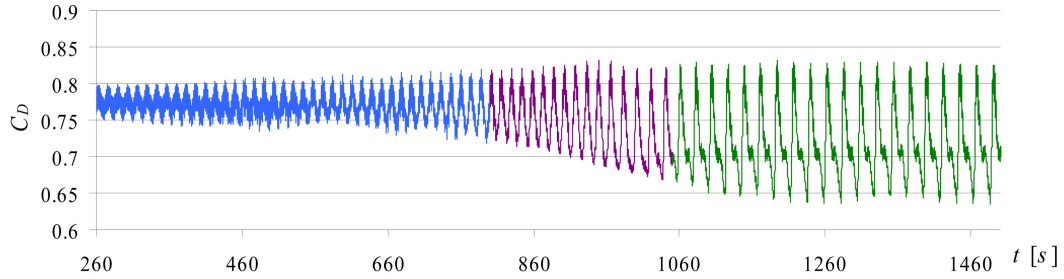

Fig. 13 Drag coefficient vs. time

amplitude increases to a certain value and remains constant once it has reached that value, according with the self-limited nature of this physical phenomenon (D'Asdia 1998). During the last period of time, the RMS value for C_L is 0.26.

Finally, the time history of the along-wind vibration of the structure and the oscillation of the drag coefficient are shown in Figs. 12 and 13, respectively. It is observed a small increase of the amplitude of the along-wind vibration of the structure and the drag coefficient oscillation due to lock-in phenomenon. For $t < 800$ s, the RMS value for C_D is 0.77 whereas for $t > 1000$ s is 0.64.

6.2 Drag amplification phenomenon

A further interesting result which can also be observed for this example, is that for higher wind speeds, the response may change, resulting in a significant increase of the drag coefficient and also in the amplitude of the oscillations. Fig. 14 shows the frequency response of the across-wind vibration of the structure versus reduced velocity for different structural damping ratios β_s. The variation of the transverse amplitude response versus the reduced velocity is plotted in Fig. 15 in linear and logarithm scale.

The analysis of the data in Figs. 14 and 15 suggest that from a certain value of the reduced velocity, the vortex-shedding frequency synchronizes with the natural frequency of the structure resulting in a large-amplitude of the transverse vibration response. This value of the reduced velocity depends on the structural damping in such a way that the smaller the structural damping is, the more quickly the large-amplitude oscillation occurs and bigger it is.

In order to explain this, the case of structural damping ratio $\beta_s = 0.075$ and $U_r = 13$ is going to be considered as representative of the rest. Figs. 16 and 17 show the oscillation of the lift coefficient and the across-wind vibration of the structure, respectively.

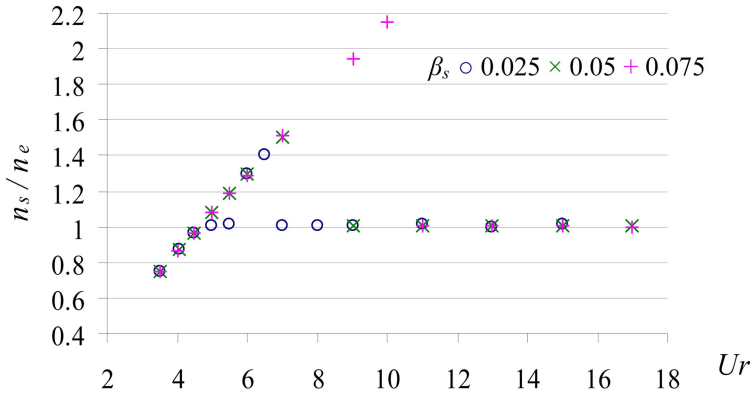

Fig. 14 Frequency response vs. reduced velocity

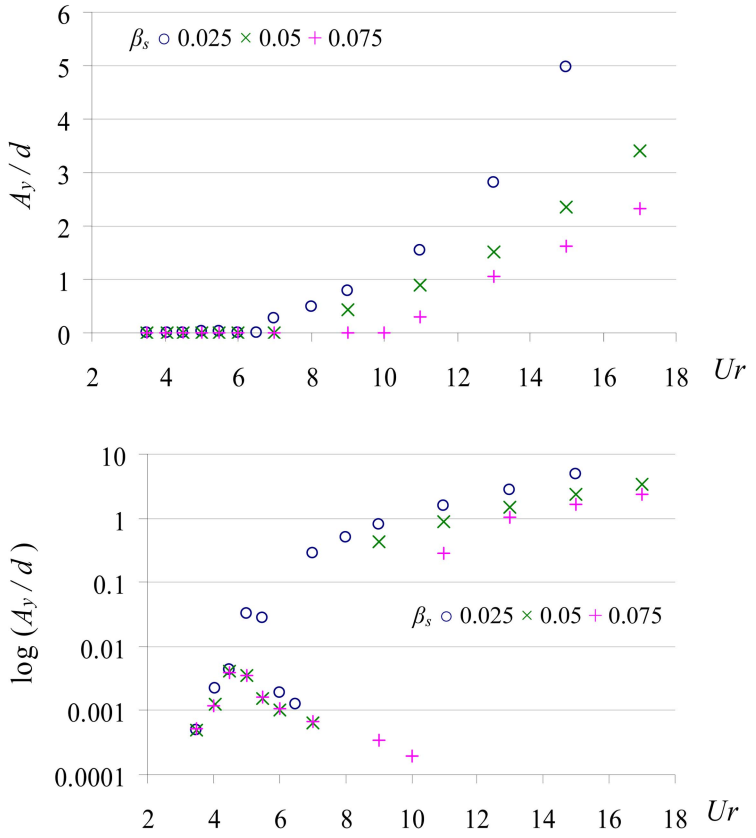

Fig. 15 Amplitude response vs. reduced velocity

During the first seconds of the analysis ($t < 250$ *s* approximately), the transverse displacements are small and the frequency of the lift coefficient is 1.2 *Hz* (Fig. 18). This value is due to the vortex shedding action and is coherent with the Strouhal relation for $St = 0.21$ ($Re = 6.67 \cdot 10^4$), so, according to Eq. (1), $n_s = 0.21*2.88/0.5 = 1.2$ *Hz*.

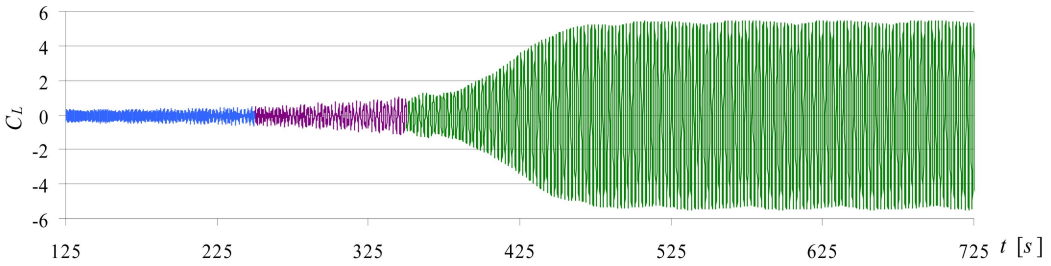

Fig. 16 Time history of lift coefficient oscillation

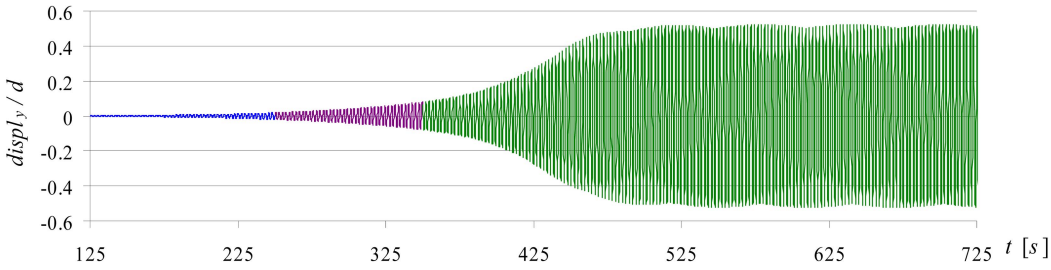

Fig. 17 Across-wind vibration of the structure

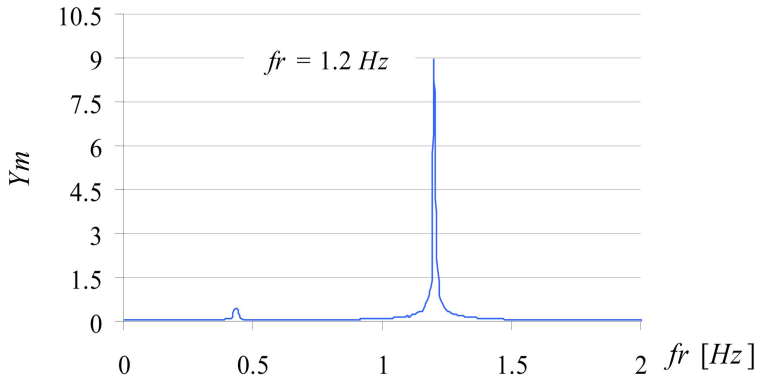

Fig. 18 PSD for C_L for $t < 250$ s

The synchronization occurs for a time t between 250 and 350 s approximately, (Fig. 19). Finally, for times $t > 350$ s, the frequency of the fluctuating lift coefficient is the natural frequency (Fig. 20), and the transverse displacements show an increment of the amplitude very important due to structural motion begins to interact strongly with the wind field and the structure's natural frequency commands the vortex-shedding phenomenon.

The along-wind response during the former exposed across-wind response is being analyzed next. Fig. 21 shows the corresponding time history. For a time $t > 350$ s, when the natural frequency of the structure synchronizes with the vortex-shedding frequency, the structure vibrates around a bigger value and also the amplitude of those vibrations is bigger comparable with the transverse vibration. There is a strong correlation between the along-wind and transverse vibrations, as the frequency of transverse vibration, 0.43 Hz (Fig. 22) is exactly half the frequency for the streamwise oscillation,

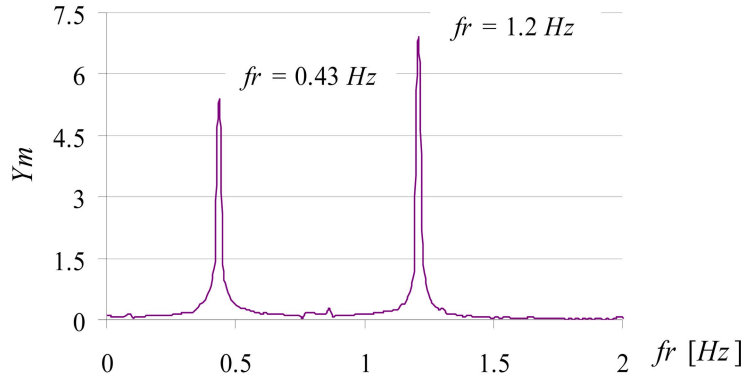

Fig. 19 PSD for C_L for $250 < t < 350$ s

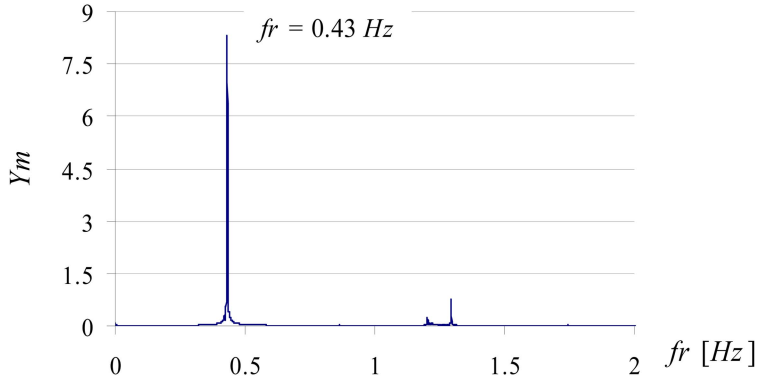

Fig. 20 PSD for C_L for $t > 350$ s

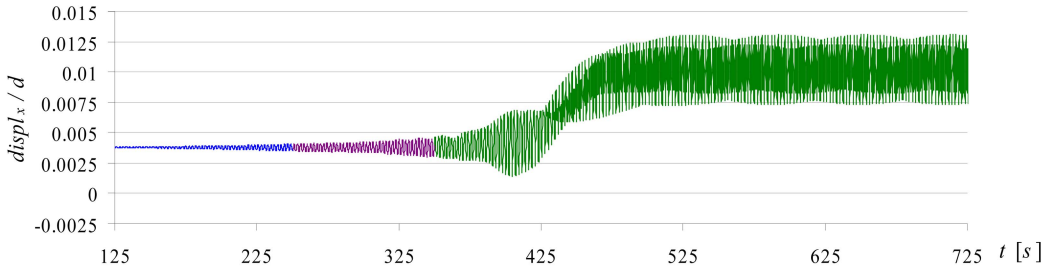

Fig. 21 Along-wind vibration of the structure

0.86 *Hz*. This is in accordance with the experimental results of Fujarra (2001).

This vibration mode is due to a coupled streamwise-transverse vibration, resulting in drag amplification as observed in Fig. 23, which shows the oscillation of the drag coefficient with time. The RMS value for $t < 250$ *s* is 0.77 and for $t > 350$ *s* is 1.78. Fig. 24 shows the PSD for the drag coefficient and it is observed that the oscillation of this coefficient occurs at the frequency of 0.86 *Hz*, which is exactly twice as much as the frequency of the oscillation of the lift coefficient.

Fig. 25 shows the RMS value of the drag as function of the reduced velocity for different structural damping ratios. It is observed that the smaller the structural damping is, the quicker the

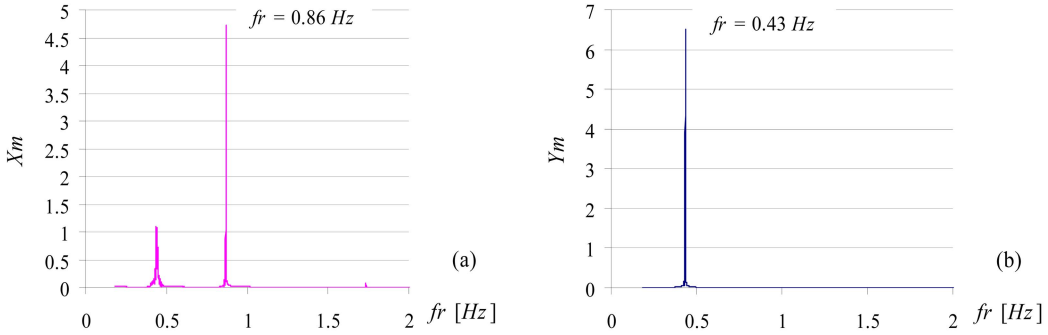

Fig. 22 PSD for the across-wind (a) and the along-wind and (b) vibration for $t > 350$ s

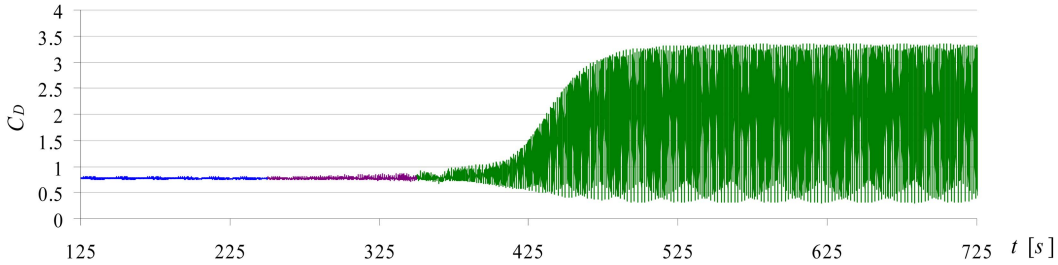

Fig. 23 Time history of drag coefficient oscillation

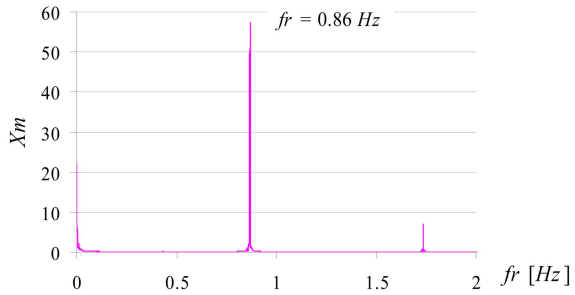

Fig. 24 PSD for C_D

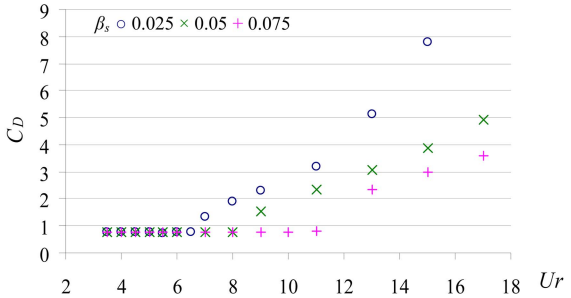

Fig. 25. RMS value of the drag coefficient vs. reduced velocity

RMS value of the drag coefficient increases from a certain value of the velocity.

The variation of the RMS value of the drag coefficient with the transverse displacement is plotted in Fig. 26 on a linear and logarithm scale, showing that the increase of the drag coefficient depends on the amplitude of the transverse vibration of the structure but it is not clear its dependency on structural damping ratio.

Finally, Fig. 27 shows the along-wind displacement of the structure versus the reduced velocity where the non linearity is clearly noticed.

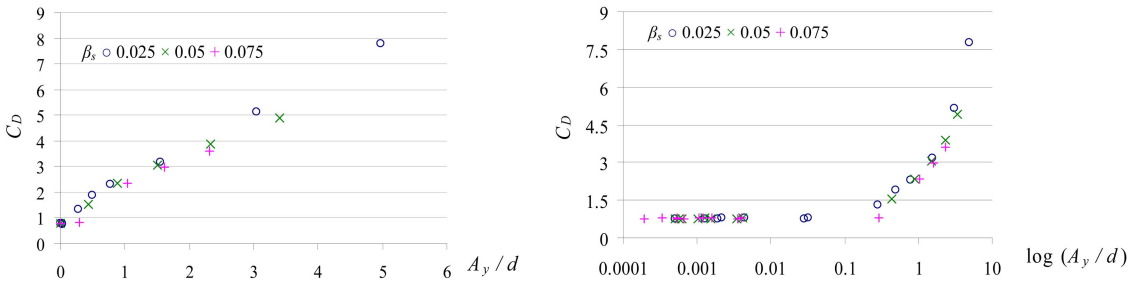

Fig. 26 RMS value of the drag coefficient vs. transverse response

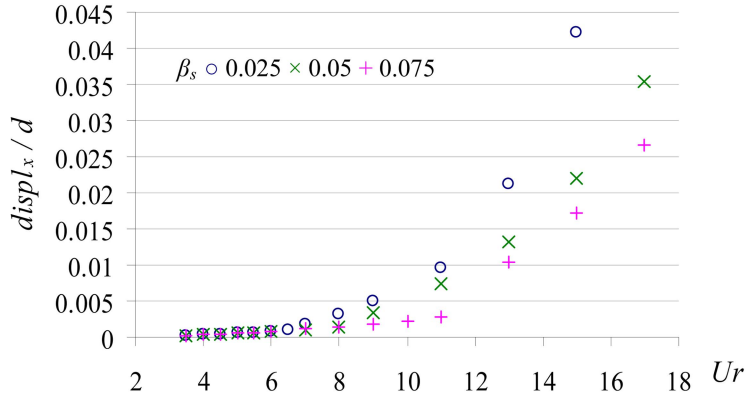

Fig. 27 RMS value of the along-wind displacement vs. reduced velocity

7. Conclusions

In summary, a simplified numerical method for the fluid-structure interaction analysis of line slender structures subjected to the action of the wind has been developed. The structural problem has been modelled with a one-dimensional element for thin walled cross-section beams, and the wind has been modelled as an incompressible fluid acting on the structure in a series of planes that are independent among them and transverse to the structure. This approximation is valid only under the hypothesis that no flow is present in the direction of the beam, applicable in particular cases (bridges or industrial chimneys, under particular winds), but may not hold in different contexts. In its simplicity, the model is well suited for providing an engineering insight in a number of different problems in civil engineering, as the one presented in this paper, where the lock-in effect and drag amplification phenomenon has been captured and compared to experimental results.

Vortex shedding frequency and the across-wind amplitude of the vibration of the structure under wind action have been plotted against the reduced velocity for different values of the structural damping. It appears that the damping of the structure has and important role in the occurrence of the phenomenon of synchronization. Time histories of the along- and across- wind response of the structure have been presented, showing changes in the vortex shedding frequency in a certain range of velocities.

The variation of the drag coefficient with the reduced velocity and the along-wind amplitude of the vibration of the structure have also been presented. A high-speed vibration mode with large-

amplitude response has been found, which is outside the principal synchronization range, and is associated with a streamwise-transverse vibration coupling. In this regime, the drag coefficient depends on the amplitude of the transverse vibration of the structure for any value of the structural damping and the frequency of the oscillation of this coefficient is twice as much as the frequency of the oscillation of the lift coefficient. Also, it is observed that the RMS value increases more quickly the smaller the structural damping is. Finally, the along-wind displacement of the structure has been plotted as function of the reduced velocity for different values of the structural damping, showing the non linearity of the problem.

This work provides new opportunities for validation of the forces induced by vortex shedding calculated by the theory of computational fluid dynamics coupled with a structural model, as well as the dynamic behaviour of the structure. In spite of the simplifying assumption that the flow on each of the planes is independent on the flow on the neighbouring ones is taken and no tip effects are considered, the use in the simulation of 2D fluid planes coupled with the structural deformation provides an interesting alternative to 3D and clearly improves the classic 2D approach.

References

Basu, R.I. and Vickery, B.J. (1983), "Across-wind vibrations of structures of circular cross-section. Part II. Development of a mathematical model for full-scale application", *J. Wind. Eng. Ind. Aerod.*, **12**(1), 75-97.

Belver, A.V. (2009), *Analysis of aeroelastic vibrations in slender structures under wind loads*, Ph.D. Dissertation, University of Valladolid, Spain.

Belver, A.V., Mediavilla, A.F., Iban, A.L. and Rossi. R. (2010), "Fluid-structure coupling analysis and simulation of a slender composite beam", *Sci. Eng. Compos. Mater.*, **17**(1), 47-77.

Bishop, R.E.D. and Hassan, A.Y. (1964), "The lift and drag forces on a circular cylinder in a flowing field", *Proceedings of the Royal Society*, London Series A 227.

Blevins, R.D. and Burton, T.E. (1976), "Fluid Forces Induced by Vortex Shedding", *J. Fluid. Eng.-T ASME*, **98**(1), 19-26.

Braza, M., Chassaing, P. and Minh, H.H. (1986), "Numerical study and physical analysis of the pressure and velocity fields in the near wake of a circular cylinder", *J. Fluid Mech.*, **165**, 79-130.

Codina, R. (2000), "Stabilization of incompressibility and convection through orthogonal sub-scales in finite element methods", *Comput. Method. Appl. M.*, **190**(13-14), 1579-1599.

Codina, R. (2001), "Pressure stability in fractional step finite element methods for incompressible flows", *J. Comput. Phys.*, **170**(1), 112-140.

Codina, R. (2002), "Stabilized finite element approximation of transient incompressible flows using orthogonal subscales", *Comput. Method. Appl. M.*, **191**(39-40), 4295-4321.

Codina, R., Principe, J. and Avila, M. (2010), "Finite element approximation of turbulent thermally coupled incompressible flows with numerical sub-grid scale modelling", *Int. J. Numer. Method. H.*, **20**(5) ,492-516.

D'Asdia, P. and Noè, S. (1998), "Vortex induced vibration of reinforced concrete chimneys: in situ experimentation and numerical previsions", *J. Wind. Eng. Ind. Aerod.*, **74-76**, 765-776.

Dadvand, P., Rossi, R. and Oñate, E. (2010), "An object-oriented environment for developing finite element codes for multi-disciplinary applications", *Arch. Comput. Method. E.*, **17**(3), 253-297.

Dawes, W.N. (1993), "Simulating unsteady turbomachinery flows on unstructured meshes which adapt both in time and space", *Proceedings of the International Gas Turbine and Aeroengine Congress and Exposition*, Cincinnati, Ohio, USA, May.

Donea, J. and Huerta, A. (2003), *Finite element methods for flow problems*, Wiley: Chichester.

Dyrbye, C. and Hansen, S.O. (1997), *Wind loads on structures*, J. Wiley & Sons, Chichester, England.

Feng, C.C. (1968), *The measurement of vortex-induced effects in flow past a stationary and oscillating circular cylinder and d-section cylinders*, Master's Thesis, Universidad de British Columbia, Vancouver, Canada.

Forster, C. (2007), *Robust methods for fluid-structure interaction with stabilized finite elements*, PhD thesis, Stuttgar.
Fujarra, A.L.C., Pesce, C.P., Flemming, F. and Williamson, C.H.K. (2001), "Vortex-induced vibration of a flexible cantilever", *J. Fluid. Struct*., **15**(3-4), 651-658.
Gorski, P. (2009), "Some aspects of the dynamic cross-wind response of tall industrial chimney", *Wind Struct*., **12**(3), 259-279.
Gorski, P. and Chmielewski, T. (2008), "A comparative study of along and cross-wind responses of a tall chimney with and without flexibility of soil", *Wind Struct*., **11**(2), 121-135.
Hansen, S.O. (1981), "Cross-wind vibrations of a 130-m tapered concrete chimney", *J. Wind. Eng. Ind. Aerod*., **8**(4-5), 145-155.
Hartlen, R.T. and Currie, I.G. (1970), "Lift-oscillator of vortex-induced vibration", *J. Eng. Mech.- ASCE*, **96**(5), 577-591.
Idelsohn, S.R., Del Pin, F., Rossi, R. and Oñate, E. (2009), "Fluid-structure interaction problems with strong addedmass effect", *Int. J. Numer. Meth. Eng*., **80**(10), 1261-1294.
Jan, Y.J. and Sheu, T.W.H. (2004), "Finite element analysis of vortex shedding oscillations from cylinders in the straight channel", *Comput. Mech*., **33**(2), 81-94.
Kalktsis, L., Triantafyllou, G.S. and Ozbas, M. (2007), "Excitation, inertia, and drag forces on a cylinder vibrating transversely to a steady flow", *J. Fluid. Struct*., **23**(1), 1-21.
Kitagawa, T., Fujino, Y. and Kimura, K. (1999), "Effects of free end condition on end-cell induced vibration", *J. Fluid. Struct*., **13**(4), 499-518.
Kwok, C.S. (1981), "Wind-induced lock-in excitation of tall structures", *J. Eng. Mech.- ASCE*, **107**(1), 57-72.
Lankadasu, A. and Vengadesan, S. (2010), "Large eddy simulation of bluff body wake in planar shear flow", *Int. J. Numer. Meth. Fl*., **64**(6), 676-688.
Lopes, A.V., Cunha, A. and Simoes, L.M.C. (2004), "Modelo computacional de análise aeroelástica das condiçoes de utilizaçao de estructuras esbeltas", *Proceedings of the Congresso de Metodos Computacionais em Engenharia*, Lisboa, Portugal, May.
Lucor, D., Imas, L. and Karniadakis, G.E. (2001), "Vortex dislocations and force distribution of long flexible cylinders subjected to sheared flows". *J. Fluid. Struct*., **15**(6), 887-887.
Mediavilla, A.F., Garcia, J.A.G. and Belver, A.V. (2007), "One-dimensional model for the analysis of thin-walled composite beams", *Rev. Int. Metod. Numer*., **23**(2), 225-242.
Meneghini, J.R., Saltara, F., Fregonesi, R.D., Yamamoto, C.T., Casaprima, E. and Ferrari, J.A. (2004), "Numerical simulations of VIV on long flexible cylinders immersed in complex flow fields", *Proceedings of the Conference on Bluff Body Wakes and Vortex-Induced Vibrations (BBVIV-3)*, European Journal of Mechanics B-Fluids, **23**(1), 51-63.
Nieto, F., Hernandez, S., Jurado, J.A. and, Baldomir A. (2010), "CFD practical application in conceptual design of a 425 m cable-stayed bridge", *Wind Struct*., **13**(4), 309-326.
Norberg, C. (2001), "Flow around a circular cylinder: aspects of fluctuating lift", *J. Fluid. Struct*., **15** (3-4), 459-469.
Oñate, E., Valls, A. and Garcia, J. (2007), "Computation of turbulent flows using a finite calculus-finite element formulation", *Int. J. Numer. Meth. Eng*., **54**(6-8), 609-637.
Prasanth, T. K., Behara, S., Singh, S.P., Kumar, R. and Mittal, S. (2006), "Effect of blockage on vortex-induced vibrations at low Reynolds numbers", *J. Fluid. Struct*., **22**(6-7), 865-876.
Prasanth, T.K. and Mittal, S. (2008), "Vortex-induced vibrations of a circular cylinder at low Reynolds numbers", *J. Fluid Mech*., **594**, 463-491.
Principe, J, Codina, R. and Henke, F. (2010), "The dissipative structure of variational multiscale methods for incompressible flows", *Comput. Method. Appl. M*., **199**(13-16), 791-801.
Repetto, M.P. and Solari, G. (2002), "Dynamic crosswind fatigue of slender vertical structures", *Wind Struct*., **5**(6), 527-542.
Rodi, W. (1997), "Comparison of LES and RANS calculations of the flow around bluff bodies", *J. Wind. Eng. Ind. Aerod*., **69-71**, 55-75.
Rossi, R. and Oñate, E. (2010), "Analysis of some partitioned algorithms for fluid-structure interaction", *Eng. Comput*., **27**(1), 20-56.

Selvam, R.P., Govindaswamy, S. and Bosch, H. (2002), "Aeroelastic analysis of bridges using FEM and moving grids", *Wind Struct*., **5**(2), 257-266.
Simiu, E. and Scanlan, R.H. (1978), *Wind effects on structures: An introduction to wind engineering*, John Wiley & Sons.
Skop, R.A. and Griffin O.M. (1975), "On a theory for the vortex-excited oscillations of flexible cylindrical structures", *J. Sound Vib*., **41**(2), 263-274.
Skop, R.A. and Luo, G. (2001), "An inverse-direct method for predicting the vortex-induced vibrations of cylinders in uniform and nonuniform flows", *J. Fluid. Struct*., **15**(6), 867-884.
Son, J.S. and Hanratty, T.J. (1996), "Numerical solution for the flow around a cylinder at Reynolds numbers of 40, 200 and 500", *J. Fluid Mech*., **35**, 369-386.
Vickery, B.J. and Basu, R.I. (1983), "Simplified approaches to the evaluation of the across-wind response of chimneys", J. *Wind. Eng. Ind. Aerod*., **14**(1-3), 153-166.
Vickery, B.J. and Basu, R.I. (1983), "Across-wind vibrations of structures of circular cross-section. Part I. Development of a mathematical model for two-dimensional conditions", *J. Wind. Eng. Ind. Aerod*., **12**(1), 49-73.
Vickery, B.J. and Clark, A.W. (1972), "Lift or across-wind response of tapered stacks", *J. Struct. Division*, **98**(1), 1-20.
Willden, R.H.J. and Graham, J.M.R. (2001), "Numerical prediction of VIV on long flexible circular cylinders", *J. Fluid. Struct*., **15**(3-4), 659-669.
Williamson, C.H.K. and Govardhan, R. (2008), "A brief review of recent results in vortex induced vibrations", *J. Wind. Eng. Ind. Aerod*., **96**(6-7), 713-735.

JH